# Functionalized Low Defect Graphene Nanoribbons and Polyurethane Composite Film for Improved Gas Barrier and Mechanical Performances

Changsheng Xiang,[†] Paris J. Cox,[‡] Akos Kukovecz,[⊥ ‖],* Bostjan Genorio,[†,#] Daniel P. Hashim,[‡] Zheng Yan,[†] Zhiwei Peng,[†] Chih-Chau Hwang,[†] Gedeng Ruan,[†] Errol L. G. Samuel,[†] Parambath M. Sudeep,[‡,▽] Zoltan Konya,[⊥,⊗] Robert Vajtai,[‡] Pulickel M. Ajayan,[†,‡,§],* and James M. Tour[†,‡,§],*

[†]Department of Chemistry, [‡]Department of Mechanical Engineering and Materials Science, and the [§]Smalley Institute for Nanoscale Science and Technology, Rice University, 6100 Main Street, Houston, Texas 77005, United States, [⊥]Department of Applied and Environmental Chemistry, University of Szeged, Rerrich B. ter 1, H-6720 Szeged, Hungary, [‖]MTA-SZTE "Lendület" Porous Nanocomposites Research Group, Rerrich B. ter 1, H-6720 Szeged, Hungary, [#]Faculty of Chemistry and Chemical Technology, University of Ljubljana, Aškerčeva cesta 5, 1000 Ljubljana, Slovenia, [▽]Department of Physics, Cochin University of Science and Technology, Cochin, Kerala, India 682022, and [⊗]MTA-SZTE Reaction Kinetics and Surface Chemistry Research Group, Rerrich Béla tér 1, H-6720 Szeged, Hungary

ABSTRACT A thermoplastic polyurethane (TPU) composite film containing hexadecyl-functionalized low-defect graphene nanoribbons (HD-GNRs) was produced by solution casting. The HD-GNRs were well distributed within the polyurethane matrix, leading to phase separation of the TPU. Nitrogen gas effective diffusivity of TPU was decreased by 3 orders of magnitude with only 0.5 wt % HD-GNRs. The incorporation of HD-GNRs also improved the mechanical properties of the composite films, as predicted by the phase separation and indicated by tensile tests and dynamic mechanical analyses. The improved properties of the composite film could lead to potential applications in food packaging and lightweight mobile gas storage containers.
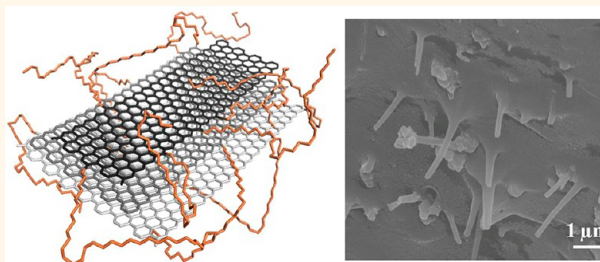
KEYWORDS: graphene nanoribbon composite · gas barrier · mechanical properties

Graphene, the two-dimensional atomically thin carbon framework, is an impermeable material,[1] in addition to its possessing intriguing electrical, mechanical and thermal properties.[2−4] Graphene can be either derived from a top-down method, such as mechanical exfoliation,[5] or from bottom-up chemical vapor deposition methods.[6−8] However, neither of the two approaches have yet been scaled to large quantities as needed for composite applications. Graphene oxide (GO), synthesized by oxidation of graphite,[9] could be used as a substitute for graphene due to its similar, though more highly oxidized structure, and its affordability and potential for synthesis on a larger scale. Pure GO and its composite films have been shown to have improved gas barrier properties.[10−15] However, the structure of GO includes many defects and holes that allow gas permeation. Furthermore, GO is unstable to water and it slowly degrades to small humic acid structures while generating acid.[16] Therefore, GO is not impermeable like graphene.

The concept of adding impermeable fillers into a polymer matrix is to create tortuous paths for the gas molecules that are attempting to travel through the film.[17] Most work to date has focused upon how the filler's aspect ratio or configuration within the polymer matrix affects gas barrier properties.[12,18] Graphene nanoribbons (GNRs) might be preferred gas barriers in composites since they, unlike GO, are stable to water, and they can be edge-funtionalized to improve processability without sacrificing the integrity of the basal planes.

In this work, we used hexadecylated GNRs (HD-GNRs) produced from *in situ* intercalation of Na/K alloy into multiwalled
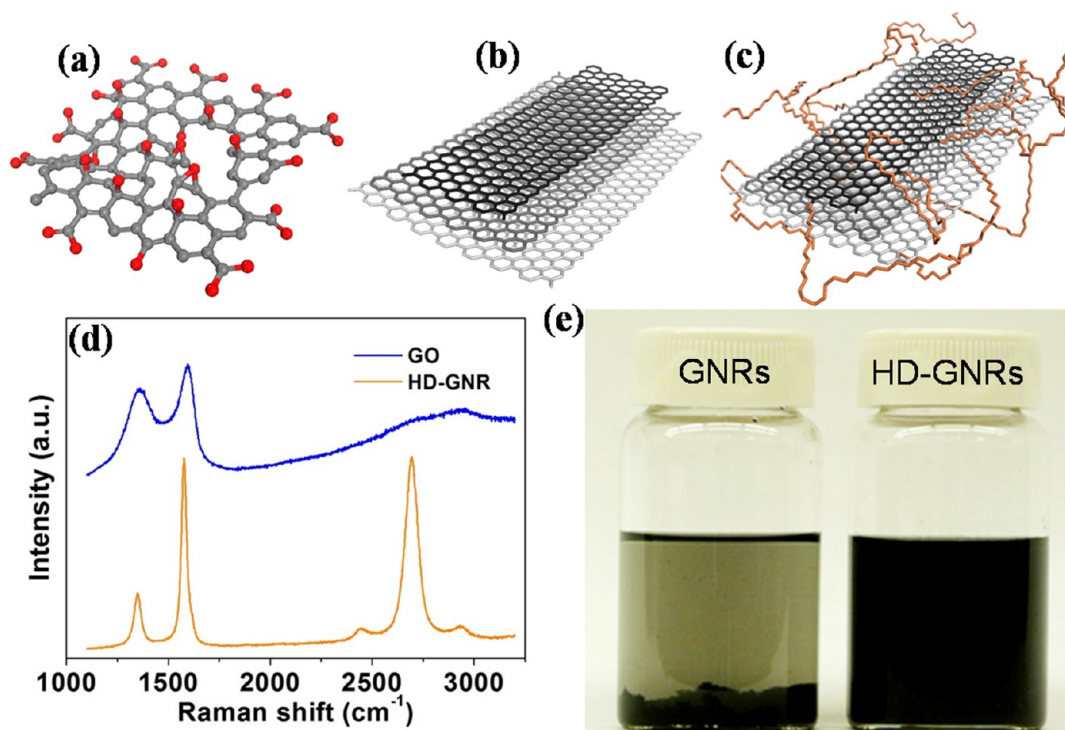
Figure 1. Chemical structure of (a) GO, (b) GNRs, (c) HD-GNRs, (d) Raman spectra of GO and HD-GNRs; (e) dispersion study of GNRs (left) and HD-GNRs (right) in chloroform (1 mg/mL).

carbon nanotubes (MWCNTS), followed by quenching with 1-iodohexadecane.[19] The hexadecyl groups on the edges make the ribbons easily dispersed in organic solvents. The resulting, somewhat foliated, HD-GNRs render the composite to be highly impermeable to gases.

Thermoplastic polyurethane (TPU) was the polymer matrix selected for the composites. TPU is comprised of linear block copolymers and is commonly used for coatings, adhesives, composites and biomedical applications.[20−22] It is synthesized from alternating hard and soft segments formed by the reaction of diisocyanates with diols.[23] The soft segments are composed of long chain polyester and polyether diols and the hard segments consist of diisocyanates and short chain extender molecules.

RESULTS AND DISCUSSION

The structures of GO, GNRs and HD-GNRs are shown in Figure 1a−c. Because of the chemical exfoliation methods for producing GO, it has a variety of oxygen functional groups and physical defects in the basal plane that can result in unwanted gas diffusion. For GNRs, the graphitic structures are mainly preserved with a low concentration of defects. However, the problem with using GNRs as nanocomposite fillers is their poor dispersion in organic solvents.[24] To address these issues, HD-GNRs were synthesized (the hexadecyl aliphatic chains are orange in Figure 1c). HD-GNRs have preserved graphitic domains with lower defect concentration than that of GO, as was confirmed by Raman spectroscopy (Figure 1d). The G/D ratio of

HD-GNRs is much higher than that of GO. In addition, the 2D peak of HD-GNRs was quite obvious, indicating good graphitic structure, but no 2D peak was observed in GO due to the defects and heavy oxidation of its basal plane. The solubility of GNRs and HD-GNRs in chloroform was tested and is shown in Figure 1e. The mixtures were the same concentration (1 mg/mL) and were sonicated for 5 min. The GNRs started to precipitate after 10 min, while the HD-GNRs were solution stable for 2 d.

As noted, the HD-GNRs were derived from MWCNTs. Scanning electron microscopy (SEM) images of MWCNTs and HD-GNRs are shown in Figure 2a,b. The flattened ribbon structures are 200−300 nm in width, a dramatic change from the MWCNTs (80 nm). Atomic force microscopy (AFM) measurement (Figure 2c) indicates the thickness of the HD-GNRs was 36 nm, showing that they remain foliated, as we have seen in the past.[19] A transmission electron microscopy (TEM) image of the HD-GNRs is shown in Figure 2d. The density of HD-GNRs is 2.1 g/cm^3.

The composite films were made by solution casting (see Materials and Methods for full procedure). Figure 3a is a cross-sectional SEM image of a TPU/5 wt % HD-GNRs composite film after sputtering 5-nm-thick gold on its surface for imaging. Figure 3b is a high resolution image of the same sample showing that the HD-GNRs are well-distributed within the TPU matrix. SEM images of TPU composite films at other HD-GNRs concentrations are shown in Supporting Information Figure S1.

Adding nanoparticles to the TPU matrix can cause a phase separation of the hard and soft segments of the
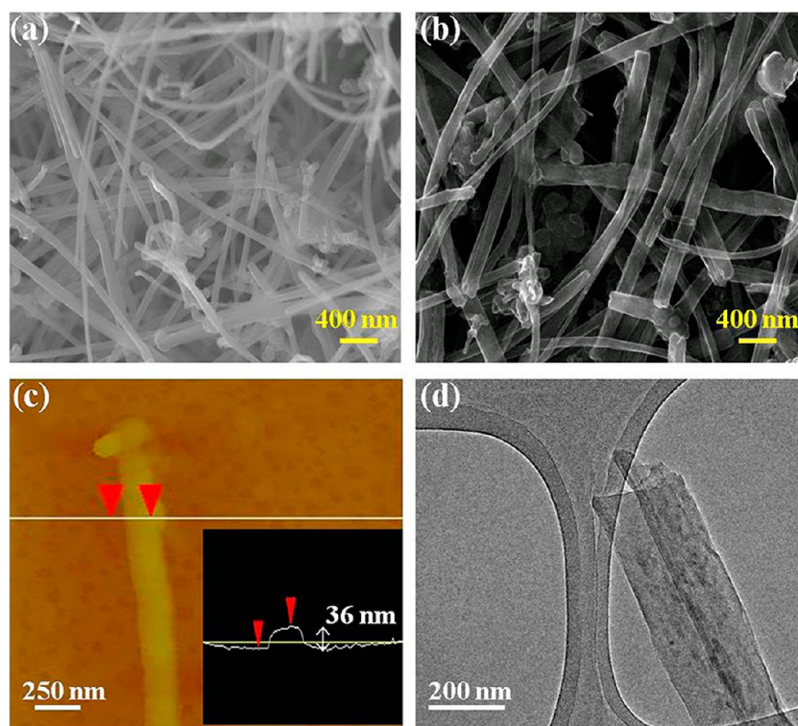
Figure 2. (a) SEM image of MWCNTs; (b) SEM image of HD-GNRs; (c) AFM image of HD-GNRs, the inset height profile indicates the vertical distance was 36 nm; (d) TEM image of stacked HD-GNRs on a copper grid.
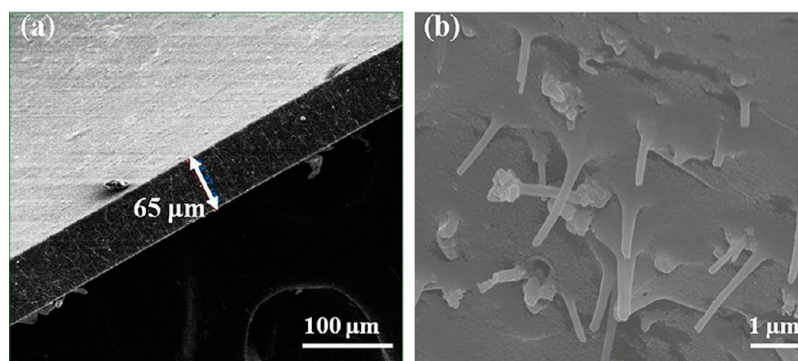

Figure 3. (a) SEM image of a cross section of TPU/5 wt % HD-GNRs film after cutting with a razor blade. (b) High resolution image of (a).

polymer due to the interdomain interface and related free energy and entropy changes.[25] This has been observed by others by their adding nanoclays,[26] carbon nanotubes[27] and GO to TPU.[12] Phase separation was also detected in this work. The most common method for characterization of TPU phase separation is by Fourier-transform infrared (FTIR) spectroscopy to observe the C=O stretching within the hard segments of TPU. These C=O can either form hydrogen bonds with the N−H groups in the hard segments or be non-hydrogen bond. The more hydrogen bonding, the higher the level of phase separation of the TPU. In the FTIR spectrum, the hydrogen bonded C=O appears at 1697 cm^{-1} while the free C=O stretching peaks at 1714 cm^{-1}. FTIR spectra of a TPU control and the composite samples are shown in Figure 4a. As the

concentration of HD-GNRs increased, the intensity ratio of hydrogen bonded C=O to free C=O increased, indicating the occurrence of phase separation.

Thermal stabilities of these composite films were characterized by thermogravimetric analysis (TGA). Interestingly, the thermal stability of TPU decreased while being heated from 250 to 340 °C and then increased from 340 to 500 °C. The decrease in thermal stability in the first temperature range may come from the thermal decomposition of HD-GNRs functional groups.[19] The HD-GNRs control sample suffered a dramatic weight loss that started at 150 °C, and reached equilibrium after 300 °C. Another reason for the weight loss may be due to phase separation. The decomposition of TPU has two stages: the hard segment decomposes in the first stage and the soft
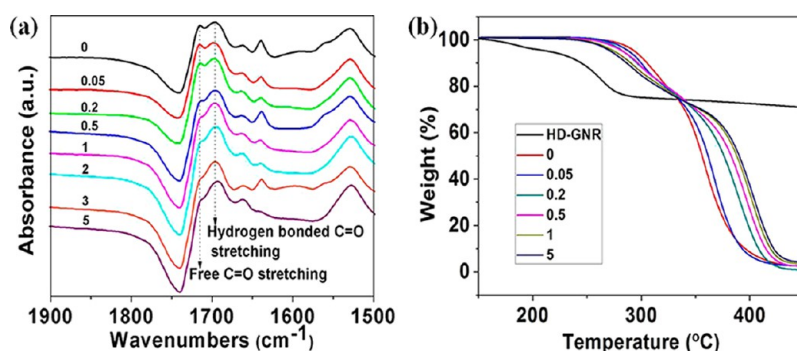
Figure 4. (a) FTIR spectra of TPU and TPU/HD-GNRs composite films. (b) TGA measurements of HD-GNRs and TPU/HD-GNRs composite films. TPU with 2 and 3 wt % HD-GNRs were eliminated from the figure since they almost overlapped with 1 and 5 wt % curves, thereby complicating the plot.
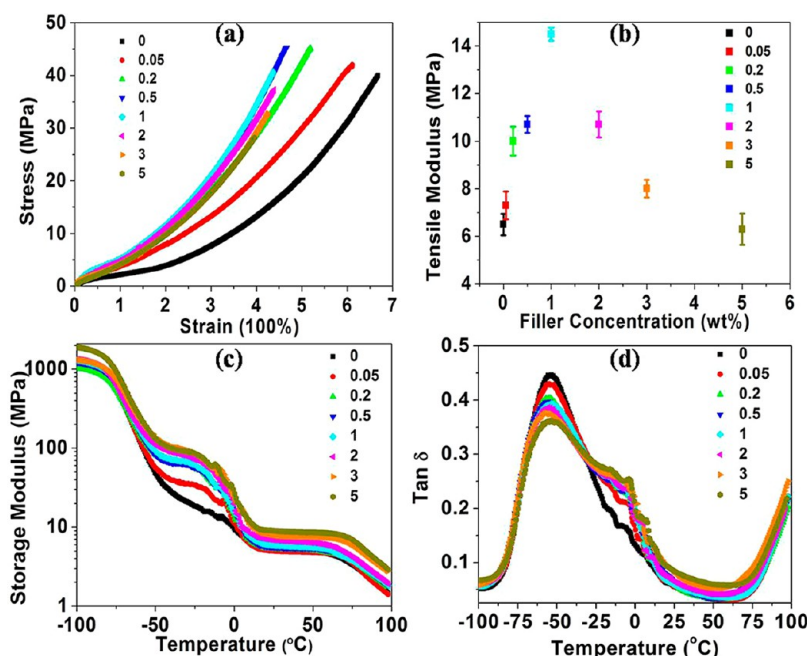

Figure 5. (a) Stress−strain curves of TPU and TPU/HD-GNRs composite films. (b) Summary of tensile moduli of different samples. (c) Storage moduli of TPU and TPU/HD-GNRs composite films as a function of temperature. (d) Damping factor (Tan δ) of TPU and TPU/HD-GNRs composite films as a function of temperature.

segment decomposes in the second stage.[28,29] When these two segments are mixed, the soft segment will have an inhibiting effect on the hard segment. However, phase separation isolates the segments and reduces the inhibiting effect, thus the thermal degradation increases as the phase separation increases in the early temperature range. In the second temperature range, the thermal stability increased at higher phase separations due to the lack of residual hard segments.

The mechanical properties of these composite films were characterized with static tensile tests and dynamic mechanical analysis (DMA). The stress−strain curves of the samples are shown in Figure 5a as a function of increasing HD-GNR weight fraction with a maximum observed at 0.5 wt % HD-GNR. Higher HD-GNR concentrations resulted in stress concentration, which led to a decrease in fracture stress.

The tensile moduli of these samples are summarized in Figure 5b, and the reinforcing effects of HD-GNRs on the modulus are similar to the stress level. The modulus increased and peaked at 1 wt % HD-GNRs, and then gradually decreased upon further filler additions. DMA testing was carried out from −100 to 100 °C, and the storage modulus with respect to the temperature is shown in Figure 5c. The improved mechanical properties of the composite films are attributed to a synergistic effect of both the incorporated HD-GNRs and the phase separation; higher HD-GNRs concentration led to higher storage modulus. Tan δ (loss modulus/storage modulus) peaks in Figure 5d deceases as more HD-GNRs was added, which means that the presence of HD-GNRs within the TPU matrix lowers damping capacity. In addition, the peaks at −60 to −50 °C are associated with the glass transition temperature (Tg) of the soft phase of the TPU. In general, adding fillers to the
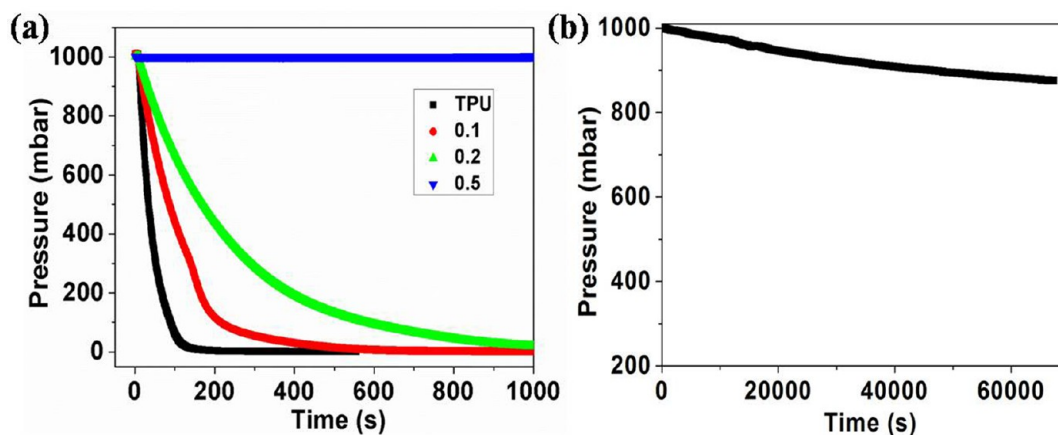
Figure 6. (a) Pressure drop of TPU and TPU/HD-GNRs films with respect to time. (b) Pressure drop of TPU/0.5 wt % HD-GNRs composite film over a longer time period.

TABLE 1. Effective Diffusivities of TPU and TPU/HD-GNRs Films

sample name	D_{eff} (10^{-6} m^2/s)
TPU	3.90
TPU/0.1 wt % HD-GNRs	1.47
TPU/0.2 wt % HD-GNRs	0.65
TPU/0.5 wt % HD-GNRs	2.97×10^{-3}

polymer matrix should shift Tg to higher temperatures because the filler would restrict local polymer motions. However, the Tg of TPU was shifted to lower temperatures while adding HD-GNRs in this work. This is because phase separation of TPU causes fewer hard segments to be alongside soft segments, so that the motion of the soft segment becomes easier. The hindering effect of hard segments plays a more important role than that of HD-GNRs in determining Tg shift; this result has been observed in TPU/carbon nanotube composites.[27]

The N$_2$ gas permeability of the TPU/HD-GNR films was characterized by measuring the time necessary for a known amount of gas at ambient conditions to diffuse through the film into a dynamic vacuum <3×10^{-3} mbar. The pressure drop was measured by a gas-type independent capacitive manometer. The reported effective diffusivities represent the average of three independent experiments for each sample, and the standard deviation was within ±5%.

The pressure drop curves of TPU and TPU/HD-GNRs composite films are shown in Figure 6a. The exponential decay function $p(t) = C + P_0 e^{-t/\tau}$ was fitted to the pressure drop curves, where $p(t)$ is the measured pressure (mbar), C is a constant, P_0 is the initial pressure in the reservoir (mbar), t is the time (s) and τ is the time constant of the pressure drop. The effective diffusivity D_{eff} (m^2/s) of the gases was calculated from the time constant according to $D_{eff} = V_u l / A\tau$, where V_u (m^3) is the volume of the gas reservoir, l (m) is the thickness of the film, and A (m^2) is the area of the film.[30]

For the TPU control sample, the total N$_2$ in the gas reservoir permeates through the film in about 100 s. When 0.1 wt % HD-GNRs was added, it took about 500 s for the N$_2$ to pass through. At 0.2 wt % HD-GNRs, the time increased to about 1000 s. Interestingly, no pressure drop was detected when TPU/0.5 wt % HD-GNRs film was tested over a period of 1000 s. This dramatic change was seen as an effect of the HD-GNRs at a threshold concentration that provides very tortur-ous paths for the N$_2$ to travel. This TPU/0.5 wt % HD-GNRs film became nearly impermeable because the pressure drop was undetectable over a short period of time under the conditions used. The pressure drop of the same sample over a longer time is shown in Figure 6b, and a pressure decrease to 875 mbar over 67 000 s was detected. Samples with HD-GNRs higher than 0.5 wt % were similarly impermeable to N$_2$ under the applied experimental conditions. The calculated D_{eff} of these composites are summarized in Table 1; with 0.5 wt % HD-GNRs, the D_{eff} of the composite film was decreased by 3 orders of magnitude when com-pared to pristine TPU film. Thereby, its permeability was decreased by at least 3 orders of magnitude (see Supporting Information for the details), which is the best gas barrier material shown in the literature, much better than that from phenyl isocyanate GO[12] (80 × decrease at 3 wt %) and nanoclays[31] (~14 × decrease at 28 wt %). The extraordinary gas barrier performance of HD-GNRs is attributed to, first, the low defect GNRs structure producing a highly impermeable material that increases the barrier efficiency; this is the main difference between HD-GNRs and GO related materials that have more defects. Second, the HD-GNRs were well dispersed in organic solvents, which led to the uniform distribu-tion within the TPU matrix. This uniform distribution of HD-GNRs created a very tortuous path for diffusion.

It is certainly possible that a monolayer, low-defect graphene sheet could be the ultimate candidate for this type of application since the aspect ratio (width/thickness) of the fillers also plays a very important role

in the gas barrier application. It has been well-known in the literature that higher aspect ratio fillers can create a more tortuous path for the diffusion gas so as to decrease the gas permeability through the composite films.[12,26] The potential for improvement by using a low-defect, monolayer graphene is discussed in the Supporting Information.

CONCLUSIONS

HD-GNRs and TPU composite films were successfully made by solution casting, with HD-GNRs uniformly distributed within the TPU matrix. The incorporation of HD-GNRs produced TPU phase separation and enhanced the mechanical properties. The composite films also demonstrate high gas barrier efficiencies at low loadings, a result attributed to the structure of the low defect HD-GNRs and their uniform dispersion. HD-GNRs are now being mass produced,[32] and these structures should have impact in commercial applications ranging from food packaging to natural gas storage in lightweight composite pressure tanks.

MATERIALS AND METHODS

Materials. Commercial biomedical grade aliphatic, poly-ether-based TPU (Tecoflex EG 80A injection grade) was purchased from the Lubrizol Corporation (Wickliffe, OH). MWCNTs were donated by Mitsui & Co. (lot no. 05072001K28). Chloroform was purchased from Sigma-Aldrich. GO was synthesized using the improved Hummer's method.[9]

Solution Casting of Composite Films. For gas permeation test samples, the total weight of the composite film was kept at 2 g at the different HD-GNRs concentrations, so the weight of TPU and HD-GNRs can be calculated accordingly. For a typical 0.1 wt % TPU/HD-GNRs composite film, HD-GNRs (2 mg) was added to chloroform (10 mL), followed by cup sonication (Cole Parmer, model 08849-00) for 5 min. TPU (1.98 g) was added to the HD-GNR solution, and the mixture was stirred for 2 h to obtain a homogeneous dispersion. The viscous solution was then poured into a homemade cylindrical steel mold (diameter = 8 cm and depth = 12 mm), and the mold was placed in a fume hood at room temperature for 10 h to allow the solvent to slowly evaporate. For mechanical testing samples, the total weight was lowered to 1 g for easier testing.

Mechanical Testing. Tensile testing was carried out using an Instron Electropuls E3000. The cross head strain rate was 100%/min. Dynamic mechanical analysis (DMA) was performed in a TA Instruments Q800 series apparatus in film tension mode. Film samples were rectangular, cut into dimensions of 15 mm × 3.5 mm × 0.08 mm. The temperature was ramped from −100 to 100 °C at a rate of 2 °C/min, 1 Hz frequency and 1% strain in air. The force track was set to 150% and the preload force at 0.01 N. Data was analyzed with TA Instruments' Universal Analysis 2000 software package.

Characterization Methods. SEM was performed on a FEI Quanta 400 high resolution field emission SEM; 5 nm Au was sputtered (Denton Desk V Sputter system) on the film surface before imaging. TEM images were taken using a 2100F field emission gun TEM with HD-GNR directly transferred onto a copper TEM grid. AFM image was obtained on a Digital Instrument Nanoscope IIIA AFM. Raman microscopy was performed with Renishaw Raman microscope using 514-nm laser excitation at room temperature. FTIR was measured using a Nicolet FTIR Infrared Microscope. TGA (Q50, TA Instruments) was carried out from 100 to 500 °C at 10 °C/min under argon. The density of HD-GNRs was calculated by using the weight of the HD-GNRs sample (0.1157 g) divided by the measured volume (0.054 cm^3), to give 2.1 g/cm^3. A Sievert-type apparatus was used to measure the volume of the HD-GNRs sample after *in situ* pretreatment at 100 °C under vacuum.

Gas Permeation Testing. The measured diameter of the films was 14.45 mm. Membrane thickness was 190 μm. Gas reservoir volume was 129 cm^3. The reported effective diffusivities represent the average of three independent experiments for each sample.

REFERENCES AND NOTES

1. Bunch, J. S.; Verbridge, S. S.; Alden, J. S.; van der Zande, A. M.; Parpia, J. M.; Craighead, H. G.; McEuen, P. L. Impermeable Atomic Membranes from Graphene Sheets. *Nano Lett.* **2008**, *8*, 2458–2462.

2. Chen, J. H.; Jang, C.; Xiao, S.; Ishigami, M.; Fuhrer, M. S. Intrinsic and Extrinsic Performance Limits of Graphene Devices on SiO$_2$. *Nat. Nanotechnol.* **2008**, *3*, 206–209.

3. Lee, C.; Wei, X.; Kysar, J. W.; Hone, J. Measurement of the Elastic Properties and Intrinsic Strength of Monolayer Graphene. *Science* **2008**, *321*, 385–388.

4. Ghosh, S.; Calizo, I.; Teweldebrhan, D.; Pokatilov, E. P.; Nika, D. L.; Balandin, A. A.; Bao, W.; Miao, F.; Lau, C. N. Extremely High Thermal Conductivity of Graphene: Prospects for Thermal Management Applications in Nanoelectronic Circuits. *Appl. Phys. Lett.* **2008**, *92*, 151911.

5. Novoselov, K. S.; Geim, A. K.; Morozov, S. V.; Jiang, D.; Zhang, Y.; Dubonos, S. V.; Grigorieva, I. V.; Firsov, A. A. Electric Field Effect in Atomically Thin Carbon Films. *Science* **2004**, *306*, 666–669.

6. Kim, K. S.; Zhao, Y.; Jang, H.; Lee, S. Y.; Kim, J. M.; Kim, K. S.; Ahn, J. H.; Kim, P.; Choi, J. Y.; Hong, B. H. Large-Scale Pattern Growth of Graphene Films for Stretchable Transparent Electrodes. *Nature* **2009**, *457*, 706–710.

7. Sun, Z.; Yan, Z.; Yao, J.; Beitler, E.; Zhu, Y.; Tour, J. M. Growth of Graphene from Solid Carbon Sources. *Nature* **2010**, *468*, 549–552.

8. Yan, Z.; Lin, J.; Peng, J.; Sun, Z.; Zhu, Y.; Li, L.; Xiang, C.; Samuel, E. L.; Kittrell, C.; Tour, J. T. Toward the Synthesis of Wafer-Scale Single-Crystal Graphene on Copper Foils. *ACS Nano* **2012**, *6*, 9110–9117.

9. Marcano, D. C.; Kosynkin, D. V.; Berlin, J. M.; Sinitskii, A.; Sun, Z.; Slesarev, A.; Alemany, L. B.; Lu, W.; Tour, J. M. Improved Synthesis of Graphene Oxide. *ACS Nano* **2010**, *4*, 4806–4814.

10. Nair, R. R.; Wu, H. A.; Jayaram, P. N.; Grigorieva, I. V.; Geim, A. K. Unimpeded Permeation of Water through Helium-Leak-Tight Graphene-Based Membranes. *Science* **2011**, *335*, 442–444.

11. Yang, Y. H.; Bolling, L.; Priolo, M. A.; Grunlan, J. C. Graphene: Super Gas Barrier and Selectivity of Graphene Oxide-Polymer Multilayer Thin Films. *Adv. Mater.* **2013**, *25*, 503–508.

12. Kim, H.; Miura, Y.; Macosko, C. W. Graphene/Polyurethane Nanocomposites for Improved Gas Barrier and Electrical Conductivity. *Chem. Mater.* **2010**, *22*, 3441–3450.

13. Kim, H. M.; Lee, J. K.; Lee, H. S. Transparent and High Gas Barrier Films Based on Poly(vinyl alcohol)/Graphene Oxide Composites. *Thin Solid Films* **2011**, *519*, 7766–7771.

14. Morimune, S.; Nishino, T.; Goto, T. Ecological Approach to Graphene Oxide Reinforced Poly(methyl methacrylate) nanocomposites. *ACS Appl. Mater. Interfaces* **2012**, *4*, 3596–3601.

15. Liu, H.; Kuila, T.; Kim, N. H.; Ku, B. C.; Lee, J. H. *In Situ* Synthesis of the Reduced Graphene Oxide-polyethyleneimine Composite and Its Gas barrier Properties. *J. Mater. Chem. A* **2013**, *1*, 3739–3746.

16. Dimiev, A.; Alemany, L. B.; Tour, J. M. Graphene Oxide. Origin of Acidity, Its Instability in Water, and a New Dynamic Structural Model. *ACS Nano* **2013**, *7*, 576–588.

17. Lape, N. K.; Nuxoll, E. E.; Cussler, E. L. Polydisperse Flakes in Barrier Films. *J. Membr. Sci.* **2004**, *236*, 29–37.

18. Bharadwaj, R. K. Modeling the Barrier Properties of Polymer-Layered Silicate Nanocomposites. *Macromelecules* **2001**, *34*, 9189–9192.

19. Genorio, B.; Lu, W.; Dimiev, A. M.; Zhu, Y.; Raji, A. R. O.; Novosel, B.; Alemany, L. B.; Tour, J. M. *In Situ* Intercalation Replacement and Selective Functionalization of Graphene Nanoribbon Stacks. *ACS Nano* **2012**, *6*, 4231–4240.

20. Xiang, C.; Lu, W.; Zhu, Y.; Sun, Z.; Yan, Z.; Hwang, C. C.; Tour, J. M. Carbon Nanotube and Graphene Nanoribbon-Coated Conductive Kevlar Fibers. *ACS Appl. Mater. Interfaces* **2012**, *4*, 131–136.

21. Woods, G. *The ICI Polyurethanes Book*; Wiley: New York, 1990.

22. Lamda, N. M. K.; Woodhouse, K. A.; Cooper, S. L. *Polyurethanes in Biomedical Applications*; CRC Press: Boca Raton, FL, 1998.

23. Bogdanov, B.; Toncheva, V.; Schacht, E.; Finelli, L.; Sarti, B.; Scandola, M. Physical Properties of Poly(ether urethanes) Prepared from Different Molar Mass Polycaprolactonediols. *Polymer* **1999**, *40*, 3171–3182.

24. Kosynkin, D. V.; Lu, W.; Sinitskii, A.; Pera, G.; Sun, Z.; Tour, J. M. Highly Conductive Graphene Nanoribbons by Longitudinal Splitting of Carbon Nanotubes Using Potassium Vapor. *ACS Nano* **2011**, *5*, 968–974.

25. Yilgor, E.; Yilgor, I.; Yurtsever, E. Hydrogen Bonding and Polyurethane Morphology. I. Quantum Mechanical Calculations of Hydrogen Bond Energies and Vibrational Spectroscopy of Model Compounds. *Polymer* **2002**, *43*, 6551–6559.

26. Pattanayak, A.; Jana, S. C. Synthesis of Thermoplastic Polyurethane Nanocomposites of Reactive Nanoclay by Bulk Polymerization Methods. *Polymer* **2005**, *46*, 3275–3288.

27. Xia, H.; Song, M. Preparatoin and Characterization of Polyurethane-Carbon Nanotube Composites. *Soft Matter* **2005**, *1*, 386–394.

28. Petrovic, Z. S.; Zavargo, Z.; Flynn, J. H.; Macknight, W. J. Thermal Degradation of Segmented Polyurethanes. *J. Appl. Polym. Sci.* **1994**, *51*, 1087–1095.

29. Grassie, N.; Zulfiqar, M. Thermal Degradation of the Polyurethane from 1,4-Butanediol and Methylene Bis(4-phenyl isocyanate). *J. Polym. Sci., Polym. Chem.* **1978**, *16*, 1563–1574.

30. Smajda, R.; Kukovecz, A.; Konya, Z.; Kiricsi, I. Structure and Gas Permeability of Multi-Wall Carbon Nanotube Buckypapers. *Carbon* **2007**, *45*, 1176–1184.

31. Herrera-Alonso, J. M.; Marand, E.; Little, J. C.; Cox, S. S. Transport Properties in Polyurethane/Clay Nanocomposites as Barrier Material: Effect of Processing Conditions. *J. Membr. Sci.* **2009**, *337*, 208–214.

32. AZ Electronic Materials: http://www.azem.com.